

QuanTest: Entanglement-Guided Testing of Quantum Neural Network Systems

JINJING SHI, Central South University, China

ZIMENG XIAO, Central South University, China

HEYUAN SHI, Central South University, China

YU JIANG, Tsinghua University, China

XUELONG LI, Institute of Artificial Intelligence (Tele AI), China

Quantum Neural Network (QNN) combines the Deep Learning (DL) principle with the fundamental theory of quantum mechanics to achieve machine learning tasks with quantum acceleration. Recently, QNN systems have been found to manifest robustness issues similar to classical DL systems. There is an urgent need for ways to test their correctness and security. However, QNN systems differ significantly from traditional quantum software and classical DL systems, posing critical challenges for QNN testing. These challenges include the inapplicability of traditional quantum software testing methods, the dependence of quantum test sample generation on perturbation operators, and the absence of effective information in quantum neurons. In this paper, we propose QuanTest, a quantum entanglement-guided adversarial testing framework to uncover potential erroneous behaviors in QNN systems. We design a quantum entanglement adequacy criterion to quantify the entanglement acquired by the input quantum states from the QNN system, along with two similarity metrics to measure the proximity of generated quantum adversarial examples to the original inputs. Subsequently, QuanTest formulates the problem of generating test inputs that maximize the quantum entanglement sufficiency and capture incorrect behaviors of the QNN system as a joint optimization problem and solves it in a gradient-based manner to generate quantum adversarial examples. Experimental results demonstrate that QuanTest possesses the capability to capture erroneous behaviors in QNN systems (generating 67.48%-96.05% more test samples than the random noise under the same perturbation size constraints). The entanglement-guided approach proves effective in adversarial testing, generating more adversarial examples (maximum increase reached 21.32%).

CCS Concepts: • **Software and its engineering** → **Software testing and debugging**; • **Computing methodologies** → **Neural networks**.

Additional Key Words and Phrases: Quantum neural network, deep neural network, adversarial testing, quantum entanglement

1 INTRODUCTION

Quantum Neural Network (QNN) is a novel type of Deep Learning (DL) system that utilizes quantum computing as the underlying computational paradigm. Driven by hybrid quantum-classical algorithms, QNN processes and computes quantum state data in quantum computers through Parameterized Quantum Circuits (PQCs) [7]. A number of quantum learning algorithms leverage inherent properties such as quantum entanglement and quantum superposition [54], exhibiting exponential advantages compared to their classical counterparts. The Harrow-Hassidim-Lloyd (HHL) quantum algorithm [24] and quantum principal component analysis [27, 40] are well-known examples that demonstrate this "quantum advantage."

Similar to classical Deep Neural Networks (DNNs), which still confront challenges related to robustness and security [20, 67], QNN systems have also shown worrisome vulnerabilities in adversarial scenarios [41, 60]. This will pose significant challenges for the future applications of QNNs in industry, especially when deployed in safety and security-critical systems, where

Authors' addresses: Jinjing Shi, Central South University, Changsha, China, 410083, shijinjing@csu.edu.cn; Zimeng Xiao, Central South University, Changsha, China, xiaozimeng@csu.edu.cn; Heyuan Shi, Central South University, Changsha, China, hey.shi@foxmail.com; Yu Jiang, Tsinghua University, Beijing, China, jy1989@mail.tsinghua.edu.cn; Xuelong Li, Institute of Artificial Intelligence (Tele AI), Beijing, China, li@nwpu.edu.cn.

erroneous behaviors could lead to catastrophic events. Therefore, the task of testing and evaluating QNN systems to uncover existing defects holds paramount importance in enhancing system security and quality. Nonetheless, research on QNN system testing is currently missing. The combination of quantum computing and deep learning brings a distinctive architecture to QNN systems, marked by substantial deviations from conventional quantum software and classical deep learning systems. Consequently, there are critical challenges in the QNN systems testing and design of corresponding evaluation metrics.

The first challenge arises from the inapplicability of traditional quantum software testing methods to QNN systems. At present, quantum software testing has gradually attracted attention within the software engineering community [3], and some quantum software testing methods targeting quantum programs have emerged recently [29, 36, 49, 52]. However, there is a fundamental distinction between traditional quantum software and QNN systems. At the physical level, a QNN system corresponds to a family of quantum circuits with variable structures and learnable parameters, rather than a fixed-scale specific circuit typically represented by traditional quantum software. At the logical level, a QNN system learns its rules autonomously from the features of data, whereas the system logic of traditional quantum software is directly specified by engineers. Therefore, these quantum software testing efforts for fixed circuits and decision logic of traditional software cannot be applied directly to QNN systems.

The second challenge is that the current testing methods and metrics for DL systems cannot be directly transferred to QNN systems. While a number of testing methodologies [16, 21, 39, 69] have recently emerged for popular DL systems such as Convolutional Neural Networks (CNNs) and Recurrent Neural Networks (RNNs), along with a variety of testing metrics based on neuron coverage [43, 57], surprise adequacy [32], and loss [70] have been proposed to appraise the quality of generated test cases, the quantum computing paradigm differs significantly from classical computing. Therefore, QNN testing is also different from classical DL testing as illustrated in Figure 1. These differences are two-fold:

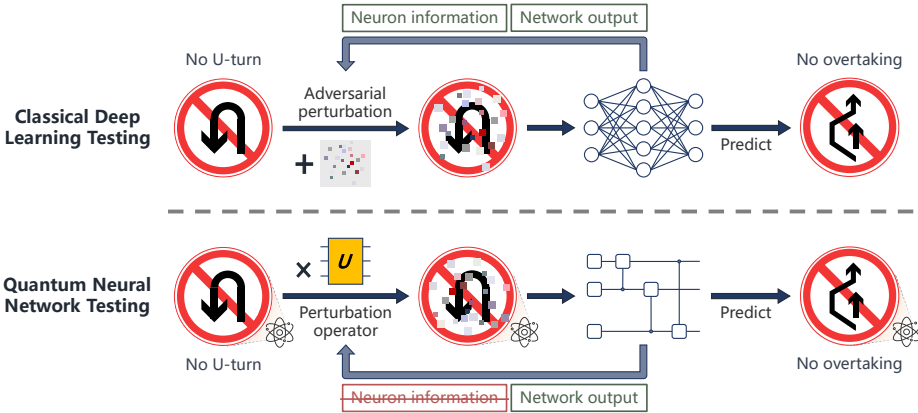


Fig. 1. The differences between classical DNN testing (upper part) and QNN system testing (lower part). In QNN system testing, the QNN components cannot extract effective neuron information as in classical DNN, and the generation of adversarial examples is also different from the classical approach.

- (1) **The approach for obtaining quantum test samples diverges from that employed in the classical world.** Due to the infinite-dimensional nature of Hilbert space, gathering

manually labeled data to trigger every feasible logic in the QNN system is extremely impractical. Moreover, in the generation of adversarial examples, classical computing can directly superimpose the original sample with the obtained perturbation in an additive manner to obtain the adversarial example. In contrast, quantum computing typically involves applying a unitary operator layer, capable of causing perturbation effects, in the form of a function on the quantum state image.

- (2) **Limited useful information can be extracted from quantum neurons.** Owing to the closed and unitary characteristics of quantum systems, apart from the parameters of rotation gates, an individual quantum neuron cannot extract more information. Valuable information often concentrates on the overall output of QNN and the corresponding measurement results. This renders existing DL testing metrics ineffective for QNN systems. Consequently, a novel evaluation metric tailored to quantum systems is imperative for QNN system testing.

In this paper, we propose QuanTest, an adversarial testing framework for QNN systems guided by quantum entanglement. It aims to generate adversarial examples that can trigger more solution spaces in QNN, thereby uncovering more erroneous behaviors in the QNN system. In particular, We first extract information from the quantum system constituted by the QNN model and quantum states. Considering the wave function collapse caused by observing the quantum systems [54], in addition to measuring the output quantum states from the QNN model to obtain predictive information, it is necessary to retain some copies for subsequent testing to calculate quantitative indicators. For the quantitative metrics, we designed an entanglement adequacy criterion to quantify the entanglement acquired by input quantum states from the QNN system and two similarity metrics to measure the proximity between the generated adversarial examples and the original inputs. Subsequently, we formulate the problem of generating test inputs that maximize quantum entanglement adequacy (QEA) of a QNN system while also exposing as many erroneous behaviors as possible as a joint optimization problem. We effectively solve this problem by obtaining perturbations in a gradient-based manner. The perturbations act directly on the original inputs in the form of a unitary operator, generating quantum adversarial examples through quantum evolution. Finally, we detect quantum adversarial examples and evaluate their quality through model performance and similarity metrics.

We implement QuanTest and conduct empirical studies on nine QNN systems, including three types each of QCL model [50], CCQC model [62], and QCNN model [13]. These models were employed to perform three classification tasks based on two popular datasets MNIST [35] and Fashion-MNIST [75]. Specifically, we first evaluated the capability of QuanTest in quantum adversarial example generation. The experimental results demonstrate that QuanTest can sensitively capture erroneous behaviors in QNN systems and generate high-quality quantum adversarial examples. Compared with random coherent noise, QuanTest can generate adversarial examples that are 67.48% to 96.05% more than random coherent noise under the same similarity constraint with fidelity measure $> 90\%$ or trace distance < 0.45 . The performance of QuanTest is better in higher-dimensional quantum systems. Furthermore, we assessed the effectiveness of entanglement guidance in adversarial testing through controlled experiments. The results indicate that entanglement guidance can lead to the generation of adversarial test inputs that trigger more solution space in QNN systems. This capability is related to the proportion of the impact of entanglement in the output quantum state in QEA.

The main contributions of this paper are summarized as follows:

- We introduce quantum entanglement adequacy as the first test adequacy metric for QNN systems, and two similarity metrics to quantify quantum state sample differences.

- We propose and implement the first quantum adversarial testing framework, QuanTest¹. QuanTest formulates the problem of both maximizing the quantum entanglement adequacy and the number of incorrect behaviors as a joint optimization problem. This is effectively solved by iteratively updating the perturbation operator.
- We evaluate the effectiveness of QuanTest through numerical simulations on nine QNN systems. The experiment results demonstrate that QuanTest can effectively detect erroneous behaviors in QNN systems and generate high-quality quantum adversarial examples under the guidance of quantum entanglement adequacy.

2 BACKGROUND

2.1 Preliminary of Quantum Computing

2.1.1 Qubits. Qubits are the quantum counterpart to classical bits in the realm of quantum computing, serving as the fundamental units of quantum computation. Unlike classical bits, which can only exist in states of 0 and 1, qubits possess unique characteristics. They can not only be in states denoted as $|0\rangle$ and $|1\rangle$ (" $|$ " represents the Dirac notation), but they can also exist in superpositions of these two states. For example, a quantum state $|\psi\rangle$ on a Hilbert space \mathbb{C}^2 can be represented as:

$$|\psi\rangle = \alpha|0\rangle + \beta|1\rangle, \quad (1)$$

where α and β are complex numbers, representing probability amplitudes and satisfying the condition $|\alpha|^2 + |\beta|^2 = 1$. $\{|0\rangle, |1\rangle\}$ consists of two orthogonal 2-dimensional state vectors and is known as the computational basis in this Hilbert space. A composite system of n qubits can be described by a unit complex vector in a 2^n -dimensional Hilbert space. Note that the quantum state space of the composite system is the tensor product of its component system's state spaces.

2.1.2 Quantum Logic Gates. The construction of quantum gates is fundamentally different from classical logic gates. In quantum circuits, any quantum gate can correspond to a unitary operator U , which is mathematically represented by a unitary matrix in terms of logic. The unitary matrix U satisfies the property of unitarity:

$$U^\dagger U = U U^\dagger = I, \quad (2)$$

where U^\dagger is the conjugate transpose of U , and I representing the identity matrix. This implies that all quantum gates must be reversible, and the dimensions of input and output must remain consistent to preserve the unitary transformation. A quantum gate acting on n qubits $|\psi\rangle$ can be described by a $2^n \times 2^n$ unitary matrix U . The essence of this operation is to perform matrix operations on the state vector, i.e., $U|\psi\rangle$. Common quantum logic gates can be categorized based on their properties and functions into fixed gates, rotation gates, and controlled gates, among others.

2.1.3 Quantum Measurement. To obtain information about the internal state of a quantum system, quantum measurements are often necessary. Measurements in quantum computing do not exist as quantum logic gates since they are irreversible. When we perform measurements on a closed quantum system, the system is no longer in a closed state, meaning it no longer follows unitary evolution. At this point, the quantum state randomly collapses onto the basis states corresponding to the Hermitian operator M associated with the measurement. Therefore, to obtain meaningful measurement results, measurements often need to be repeated multiple times.

¹<https://github.com/am0x00/QuanTest>

2.1.4 Quantum Entanglement. In a composite system, a quantum state that cannot be written as the tensor product of its component systems states is referred to as an entangled state. Entanglement can be generated through the interaction between particles, a property that is independent of the distance between the particles. In quantum computing, entanglement is often created by applying controlled gates (including CNOT, iSWAP, etc.) to qubits. Bell states (such as $(|00\rangle + |11\rangle)/\sqrt{2}$) are the maximally entangled quantum states of two qubits [54]. Entanglement is a unique resource of quantum mechanics that plays a crucial role in quantum computing and quantum information.

2.2 Quantum Neural Network

Quantum neural networks (QNNs) are a type of neural network model based on quantum computing, with the core being parameterized quantum circuits (PQCs) [7] driven by variational quantum algorithms [12]. Similar to classical feedforward neural networks, QNNs learn by updating the trainable parameters of rotation gates within the circuits through gradients—this aspect is executed by classical optimizers, and the processing and computation of the target quantum state are carried out by quantum computers. An example of using a QNN model $\mathcal{M}(|\mathbf{x}\rangle; U_{\Theta})$ for machine learning tasks is shown in Figure 2. The training data \mathbf{x} is first encoded as quantum states $|\mathbf{x}\rangle$. Subsequently, these states are input into the QNN for computation. The trainable parameters Θ within the PQC U_{Θ} are updated using classical optimizers until the results meet the expected termination criteria. In this process, the PQC U_{Θ} can be regarded as a unitary operator, and its action on the quantum state $|\mathbf{x}\rangle$ can be represented as $U_{\Theta}|\mathbf{x}\rangle$. The final output of the QNN can only be obtained after measuring $U_{\Theta}|\mathbf{x}\rangle$.

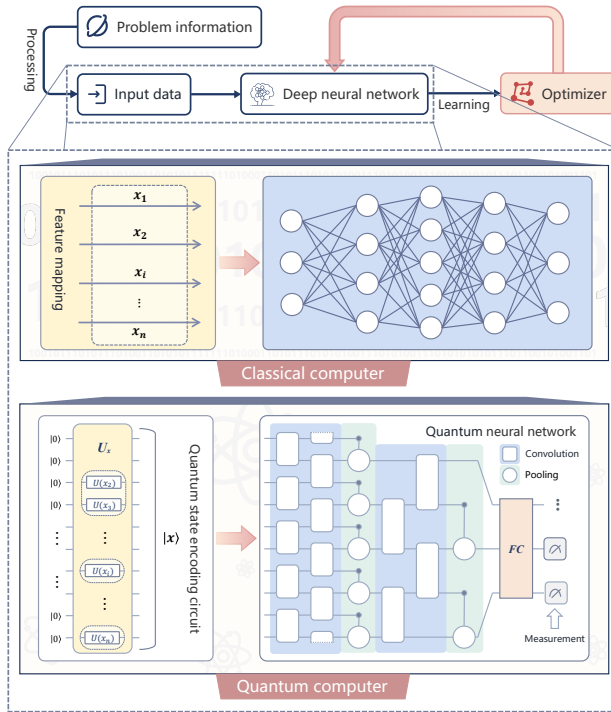


Fig. 2. Differences between QNN and classical DNN during the training process.

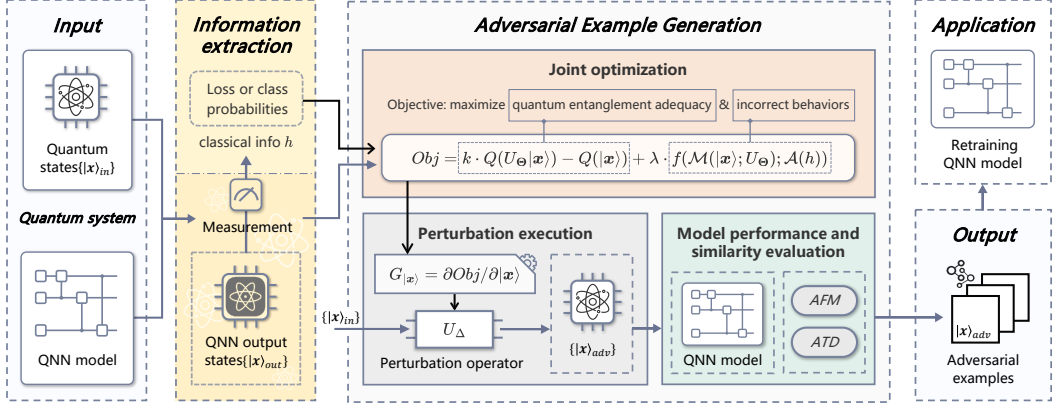


Fig. 3. Overview of the Quantest framework. Quantest takes a quantum system composed of quantum states containing classical input information and a pre-trained QNN model as input. It extracts information generated by the quantum system. Based on this information, Quantest is capable of generating quantum test samples that are adequately entangled with the QNN while inducing erroneous behaviors in the QNN system. In the diagram, black open arrows refer to the flow of classical information while the gray-blue arrows refer to the flow of quantum information.

As described in Section 2.1, the operations performed by quantum neurons as quantum gates are linear and unitary. Therefore, although the learning framework for performing tasks is similar, there are still many differences between the construction of QNNs and feedforward neural networks: the number of quantum neurons in each layer of the network is strictly limited by the number of qubits, and due to the noise in noisy intermediate-scale quantum (NISQ) devices, the scale of QNNs that current quantum computing devices can load is often limited in depth and width. Currently, QNN has given rise to various variants, including quantum convolutional neural networks (QCNNs) [13] and quantum recurrent neural networks (QRNNs) [6], among others. Novel network architectures are still being continuously proposed.

3 DESIGN

In this section, we provide an overview of our adversarial testing framework, Quantest. Figure 3 shows the workflow of Quantest.

In the information extraction module, Quantest utilizes quantum measurements to extract information generated during the quantum evolution of quantum states in the QNN model. For instance, classical information such as loss and class probabilities, which are used for adversarial attacks, needs to be measured from the quantum states outputted by the QNN model and then obtained through computation. In addition, in actual experiments, the calculation of a series of metrics designed based on quantum properties, such as the entanglement degree of quantum states and measures of similarity between quantum states, also often requires measurements of the quantum states. Considering the inherent closed nature of quantum systems that inevitably leads to the collapse of the wave function upon direct observation of quantum states [54], at this stage, Quantest additionally retains a portion of the copies of quantum states input and output from the QNN model for subsequent calculations of QEA and similarity evaluation.

Adversarial example generation is the core component of Quantest, comprising three modules: joint optimization, perturbation execution, and quality evaluation for adversarial examples. Quantest increases the model loss or the probability of target classes based on the performed

quantum-adapted adversarial attack strategy, enabling QuanTest to search for adversarial examples in a lightweight and scalable manner. Meanwhile, QuanTest also aims to enhance the entanglement of generated adversarial examples during the testing process for a more comprehensive coverage of the solution space of QNN system. Specifically, QuanTest combines the maximization of incorrect behaviors and QEA into a joint optimization problem, employing a gradient-based algorithm for effective solution. Note that, unlike typical metrics such as neuron coverage, the calculation of QEA does not originate from classical information with gradients directly extractable from QNN models. Moreover, the measure of quantum entanglement is complex and non-unique, making the design of a suitable metric for assessing entanglement adequacy crucial. We discuss key insights into the entanglement adequacy in the subsequent Section 4.2.

Based on the perturbations obtained from the solution, QuanTest independently modifies each component of the input state vector and normalizes the modified input to ensure that it still represents a quantum state in the quantum world. In the quantum circuit, this modification takes the form of a perturbation operator directly acting on the original input quantum state. Without the need for additional domain constraints, the original input can evolve into quantum adversarial examples through the perturbation operator. The construction of the perturbation operator is not rigid; it can be any unitary transformation close to the identity operator. Finally, these quantum adversarial examples are evaluated based on the performance of the tested model and similarity to the original samples to ensure the quality of the testing. The generated adversarial example set can be used for applications such as retraining to enhance the robustness of the tested model.

3.1 Quantum Entanglement Adequacy Metrics

In classical DL systems, acquiring the weights and outputs of each neuron within the DNN is straightforward. However, QNNs differ in this regard. Quantum neurons are essentially quantum logic gates represented in the form of unitary operators, making it impossible to access the output values of any individual quantum neuron in the network. This implies it is currently challenging to select specific quantum neurons and judge their coverage in the testing. To intuitively measure the adequacy of QNN system testing and better guide the generation of test samples, we consider introducing the concept of entanglement in quantum computing.

One core reason quantum computation can demonstrate potential quantum advantage in many problems is that it can construct an exponentially large quantum state space through controllable entanglement and interference [25]. By utilizing low-depth circuits to generate quantum states with high entanglement characteristics, QNN models may produce atypical patterns that classical models cannot effectively produce. These patterns can efficiently represent solution space for tasks such as prediction and classification, capturing nontrivial correlations in the data [62]. Quantum machine learning models such as quantum circuit learning (QCL) [50], parameterized Hamiltonian learning (PHL) [65], and quantum kernel methods [59] achieve strong entanglement in quantum circuits for enhancing the entanglement capability of QNNs by incorporating various configurations of multi-qubit gates such as CNOT, iSWAP, and their extended variants. We can perceive that, as the quantum state used as a test input undergoes computation within a QNN, the more adequately it activates entangled neurons, the higher the entanglement degree it obtained from the QNN. This leads to a more comprehensive coverage of the solution space in the QNN. Therefore, we propose a method to calculate the QEA of QNNs. This is achieved by measuring the entanglement of both the test input quantum state and the resulting output quantum state after undergoing unitary operations within the QNN. The difference in measurement outcomes is used to represent the QEA of that particular test case.

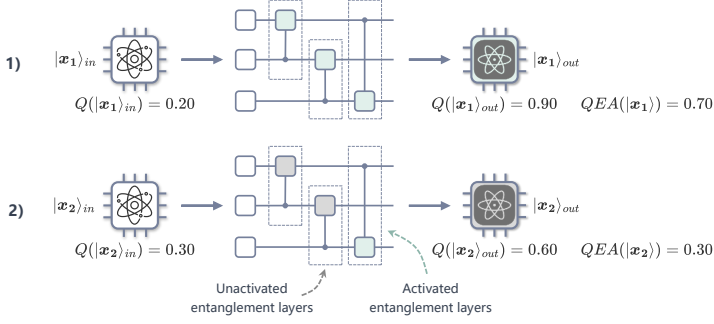


Fig. 4. The example of QEA computation for two quantum states in the QNN. The nodes in gray denote quantum entanglement layers that are not sufficiently activated, while aqua nodes represent those that are adequately activated.

Definition 1 (Quantum entanglement adequacy, QEA). Given a fully trained QNN model \mathcal{M} and a test input set $\mathcal{T} = \{\mathbf{x}_1, \mathbf{x}_2, \dots\}$, the of \mathcal{M} on the input quantum state $|\mathbf{x}\rangle$ can be equivalently represented as the multiplication of $|\mathbf{x}\rangle$ and a unitary matrix U_{Θ} , where $|\mathbf{x}\rangle$ represents the quantum state that encodes the information of $\mathbf{x} \in \mathcal{T}$, and Θ represents the learned and fixed gate parameters in \mathcal{M} . Note that the result output of $U_{\Theta}|\mathbf{x}\rangle$ is a quantum state with the same dimension as $|\mathbf{x}\rangle$. Then, the quantum entanglement adequacy (QEA) can be expressed as:

$$QEA(\mathcal{T}, \mathcal{M}, k) = \frac{1}{|\mathcal{T}|} \sum_{\mathbf{x}_i \in \mathcal{T}} |k \cdot Q(U_{\Theta}|\mathbf{x}_i) - Q(|\mathbf{x}_i)\rangle|, \quad (3)$$

where $Q(|\mathbf{x}\rangle)$ represents the MW entanglement measure for $|\mathbf{x}\rangle$, and k is used to adjust the weight of $Q(U_{\Theta}|\mathbf{x})$, in order to avoid imbalance in QEA calculations caused by the concentration of $Q(U_{\Theta}|\mathbf{x})$ at higher values when the entanglement capability [66] of QNN is strong.

For the specific calculation of Q , there are several methods currently available for quantifying entanglement as a resource. Considering that the selected measurement approach should possess a certain degree of scalability and computational simplicity, to facilitate the formulation of a guiding optimization objective, in this paper, we adopt a polynomial global measure for multipartite entanglement, known as the Meyer-Wallach (MW) entanglement measure [48]. The MW entanglement measure is defined as follows. For an n -qubit quantum system on the Hilbert space \mathbb{C}^{2^n} , define a linear map $\iota_j(b)$ that acts on the computational basis $|b_1 \dots b_n\rangle$:

$$\iota_j(b)|b_1 \dots b_n\rangle = \delta_{bb_j}|b_1 \dots \widehat{b}_j \dots b_n\rangle, \quad (4)$$

where $b \in \{0, 1\}$, \widehat{b}_j denotes the absence of the j -th qubit, and δ_{ij} is the Kronecker delta. Through the map, a new Hilbert space $\mathbb{C}^{2^{n-1}}$ can be obtained. For $|u\rangle, |v\rangle \in \mathbb{C}^{2^{n-1}}$ with $|u\rangle = \sum u_i|i\rangle$ and $|v\rangle = \sum v_i|i\rangle$, the area of the parallelogram S they form in this Hilbert space is defined as:

$$S(|u\rangle, |v\rangle) = \sum_{i < j} |u_i v_j - u_j v_i|^2. \quad (5)$$

Finally, for $|\mathbf{x}\rangle \in \mathbb{C}^{2^n}$, the MW entanglement measure Q is:

$$Q(|\mathbf{x}\rangle) = \frac{4}{n} \sum_{j=1}^n S(\iota_j(0)|\mathbf{x}\rangle, \iota_j(1)|\mathbf{x}\rangle), \quad (6)$$

where $4/n$ factor serves the purpose of normalization. The value range of $Q(|x\rangle)$ is $[0, 1]$. The larger the value of Q , the higher the degree of entanglement possessed by the quantum state. For instance, in the case of a pure state $|\phi_1\rangle = |00\rangle$, $Q(|\phi_1\rangle) = 0$, indicating the absence of entanglement. On the other hand, for a Bell state $|\phi_2\rangle = (|00\rangle + |11\rangle)/\sqrt{2}$, $Q(|\phi_2\rangle) = 1$, signifying complete entanglement.

We show the computation process of QEA using Figure 4 as an example. Quantum state data undergo entanglement measurements during the input and output of the QNN. The more entangled neurons activated by the quantum state, the greater the entanglement properties obtained. The difference between entanglement measurements before and after, i.e., the QEA, is consequently higher.

Algorithm 1 Adversarial Example Generation Guided by Entanglement

Input: inputs \leftarrow classic original inputs
 qnn \leftarrow QNN model under test
 strategy \leftarrow strategy for quantum adversarial example generation
 w \leftarrow weight of entanglement adequacy in the joint goal
 k \leftarrow parameter to balance the entanglement of input states and output states
 r \leftarrow step size in gradient ascent

Output: adversarial test input set S_{adv}

- 1: $S_{adv} = []$
- 2: **for** each $x \in$ inputs **do**
- 3: $|x\rangle = \text{encoding}(x)$; //quantum state encoding
- 4: $|x\rangle_{adv} = \text{encoding}(x)$; //copy of $|x\rangle$ for subsequent quantum adversarial example generation
- 5: $y_{ori} = \text{qnn}(|x\rangle).\text{measurement}()$; //prediction lable obtained by observing quantum system
- 6: **while** True **do**
- 7: $|x\rangle_{out} = \text{qnn}(|x\rangle_{adv})$; // output quantum state
- 8: obj_join = [];
- 9: obj_joint.append(obj_incorrect($|x\rangle_{out}$, strategy));
- 10: obj_joint.append(w · obj_entanglement($|x\rangle_{adv}$, $|x\rangle_{out}$, k));
- 11: $G_{|x\rangle_{adv}} = r \cdot \partial \text{obj} / \partial |x\rangle_{adv}$; //perturbation operator with gradient information
- 12: $|x\rangle_{adv} = \text{PERTURBATION_OP}(|x\rangle_{adv}, G_{|x\rangle_{adv}})$; //quantum adversarial examples obtained
- 13: s = measure_similarity($|x\rangle$, $|x\rangle_{adv}$);
- 14: $y_{adv} = \text{qnn}(|x\rangle_{adv}).\text{measurement}()$;
- 15: **if** $y_{adv} \neq y_{ori}$ and s meets the expectation **then**
- 16: $S_{adv}.\text{append}(|x\rangle_{adv})$;
- 17: **break**;
- 18: **end if**
- 19: **end while**
- 20: **end for**
- 21: **function** PERTURBATION_OP($|x\rangle_{adv}$, $G_{|x\rangle_{adv}}$)
- 22: **for** each $x_i \in |x\rangle_{adv}$ **do**
- 23: $\Delta = x_i + G_{x_i}$
- 24: $x_i^* = x_i + \Delta$
- 25: **end for**
- 26: **return** $|x^*\rangle_{adv}$
- 27: **end function**

3.2 QuanTest Algorithm

In this section, we describe the details of how QuanTest solves the joint optimization problem of maximizing incorrect behaviors and QEA through gradient ascent to generate adversarial examples as test inputs. Guided by entanglement, the adversarial examples generated by QuanTest are expected to trigger a broader solution space within the QNN system to discover more erroneous behaviors.

The specialized characteristics of quantum computation necessitate that QuanTest constantly considers a good fit with quantum systems in algorithm implementation and metric design, ensuring efficient execution of scalable automated testing on quantum computing devices. Algorithm 1 presents the core process of adversarial example generation guided by entanglement. Below, we discuss the specific details of the algorithm and solutions to relevant quantum challenges around three key components of the algorithm.

3.2.1 Joint Optimization. For most classical deep learning systems, the gradient of the objective function can be efficiently computed when the weight parameters and intermediate neuron values of the pre-trained DNN are transparent. QNN systems based on the same classical optimizer also share similar characteristics in gradient computation. As described in Section 2.2, QNN completes machine learning tasks by updating the learnable parameters of quantum logical gates in the PQC. Since QuanTest has access to the parameters of quantum neurons in the QNN, it can efficiently compute the gradient of the optimization objective when the parameters of the PQC are constants and the input quantum state is variable.

The optimization objective of QuanTest is defined by the following equation:

$$Obj = k \cdot Q(U_{\Theta}|x\rangle) - Q(|x\rangle) + \lambda \cdot f(\mathcal{M}(|x\rangle; U_{\Theta}); \mathcal{A}). \quad (7)$$

It consists of two parts, where the first part $k \cdot Q(U_{\Theta}|x\rangle) - Q(|x\rangle)$ is to generate test inputs that maximize QEA, and the second part $f(\mathcal{M}(|x\rangle; U_{\Theta}); \mathcal{A})$ is to generate test inputs that trigger as many incorrect behaviors in the QNN as possible. The hyperparameter λ is used to balance the two optimization objectives during the joint optimization process. We treat these two parts as a joint optimization problem and maximize this objective function (Algorithm 1 line 8-11).

- **Maximizing quantum entanglement adequacy.** QuanTest utilizes the proposed QEA metric to guide the generation of adversarial examples, thereby more comprehensively exploring the solution space of QNN. As described in Section 3.2, due to the difficulty in determining the specific state of a single quantum neuron, we assess the adequacy of the entanglement obtained from the QNN by separately measuring the entanglement degree of the quantum state before and after passing through the QNN. Unlike optimization objectives such as neuron coverage, which directly reflect the model’s state and are easy to obtain gradients, QEA indirectly captures the state of the QNN model based on the nature changes of quantum data, and the calculation of entanglement metric Q is more complex. The favorable properties of the MW entanglement measure ensure that QuanTest can effectively compute gradients for QEA, allowing QuanTest to directly use QEA as an optimization objective.
- **Maximizing incorrect behaviors.** Modular construction enables QuanTest to conveniently select different quantum-adapted adversarial attack strategies \mathcal{A} . The determination of this strategy dictates the prediction information to be further calculated after measuring the output quantum state during the information extraction. For instance, the quantum-adapted FGSM strategy requires providing loss, while the quantum-adapted DLFuzz strategy needs category probabilities as input. QuanTest aims in this section to modify the input in the form of adversarial attacks, leading the model to exhibit incorrect behavior.

All terms of the jointly optimized objective are differentiable. QuanTest can iteratively modify the input $|\mathbf{x}\rangle$ by using gradient ascent to maximize these terms. The computed gradient $\frac{\partial Obj}{\partial |\mathbf{x}\rangle}$ will become the perturbation, which is subsequently transformed into a perturbation operator on a quantum circuit for generating adversarial examples.

3.2.2 Perturbation Execution. Due to its fundamentally different computational paradigm compared to classical computing, the original quantum state cannot be simply superimposed with perturbations in an additive manner to obtain adversarial examples. This direct superposition has the potential to disrupt the unitarity of the quantum system. In practice, QuanTest independently modifies each component in the state vector and normalizes the modified state vector when necessary to ensure that it still represents a quantum state in the quantum world (Algorithm 1 line 12 and function PERTURBATION_OP). In quantum circuits, this perturbation can be achieved by constructing a perturbation operator that acts directly on the original quantum state and has a sufficiently large search space, as shown in the lower half of Figure 1. The perturbation operator does not have a fixed construction form; a simple local unitary transformation-based perturbation operator may not have a sufficiently large search space to find the target solution, while complex global operations require extremely high precision and cost. Additionally, the perturbation operator is constrained to approach the identity operator to maintain the perturbation reasonably small.

3.2.3 Quality Evaluation. The generated quantum adversarial examples need to undergo quality evaluation in terms of model performance and similarity before being output (Algorithm 1 line 13-15). Regarding the similarity evaluation of image data that has already been encoded into quantum states, we cannot directly employ classical methods to measure the difference or closeness between two input vectors. Serving as quantum generalizations of the classical notions, fidelity [31] and trace distance [26], which are two frequently utilized distance measures for quantum information, can assist us in efficiently calculating perturbations that fool the QNN system. As a result, we introduce the definitions of Average Fidelity Measure (AFM) and Average Trace Distance (ATD) to quantitatively assess the similarity between two quantum states, thereby evaluating the quality of the generated test samples. In fact, these metrics can also be effectively employed to assess the robustness of the model.

Definition 2 (Average fidelity measure, AFM). We obtain the AFM for the QNN model \mathcal{M} by calculating the sample mean of fidelity between the original inputs in \mathcal{T} and their corresponding adversarial inputs. More formally:

$$AFM(\mathcal{M}) = \frac{1}{|\mathcal{T}|} \sum_{\mathbf{x}_i \in \mathcal{T}} F(|\mathbf{x}_i\rangle\langle\mathbf{x}_i|, |\mathbf{x}_i\rangle_{adv}\langle\mathbf{x}_i|_{adv}), \tag{8}$$

where $|\mathbf{x}_i\rangle_{adv} = U_\psi|\mathbf{x}_i\rangle$, U_ψ is a perturbation operator acting on $|\mathbf{x}_i\rangle$, and $F(\rho, \sigma)$ is the fidelity between quantum state ρ and σ . Since ρ and σ are density matrices, $|\mathbf{x}_i\rangle$ and $|\mathbf{x}_i\rangle_{adv}$ should also be transformed from state vectors representation to their density matrix representation $|\mathbf{x}_i\rangle\langle\mathbf{x}_i|$ and $|\mathbf{x}_i\rangle_{adv}\langle\mathbf{x}_i|_{adv}$, respectively. $\langle\mathbf{x}_i|$ is the vector dual to $|\mathbf{x}_i\rangle$. The fidelity is defined as:

$$F(\rho, \sigma) = \text{tr}\sqrt{\sqrt{\rho}\sigma\sqrt{\rho}} = |\langle\psi_\rho|\psi_\sigma\rangle|^2. \tag{9}$$

Figure 5 shows the visualization of fidelity between two quantum states based on POVM measurements. The minimum overlap area of the probability distributions corresponding to two quantum states obtained through POVM measurements can intuitively reflect the fidelity between them. The greater the area, the higher the fidelity.

Definition 3 (Average trace distance, ATD). Similar to AFM, we define ATD as the average trace distance between the original and adversarial quantum samples. More precisely (More explicitly),

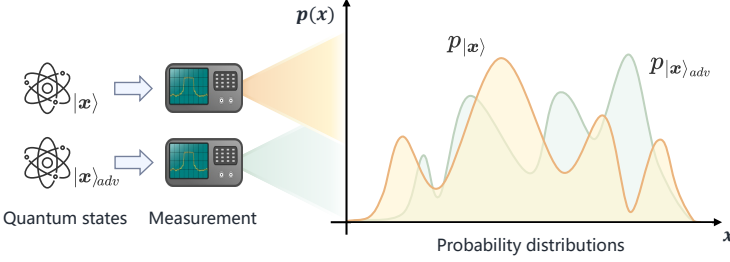


Fig. 5. Illustration of fidelity visualization between the original quantum sample $|\mathbf{x}\rangle$ and quantum adversarial example $|\mathbf{x}\rangle_{adv}$. The light orange and light green curves represent the probability distributions $p_{|\mathbf{x}\rangle}$ and $p_{|\mathbf{x}\rangle_{adv}}$ obtained through POVM measurements for the original sample and adversarial example, respectively.

the ATD is defined as:

$$ATD(\mathcal{M}) = \frac{1}{|\mathcal{T}|} \sum_{\mathbf{x}_i \in \mathcal{T}} D(|\mathbf{x}_i\rangle\langle \mathbf{x}_i|, |\mathbf{x}_i\rangle_{adv}\langle \mathbf{x}_i|_{adv}), \quad (10)$$

where $D(\rho, \sigma)$ is the trace distance between density operator ρ and σ , which is calculated as follows:

$$D(\rho, \sigma) = \frac{1}{2} \text{tr}|\rho - \sigma|. \quad (11)$$

Quantum trace distance can be regarded as a generalization of classical trace distance. In fact, during simulation calculations, the results of the quantum trace distance and the L_1 distance are often very close to each other.

4 EVALUATION

We implemented QuanTest² using the deep learning framework PaddlePaddle [45], which includes the quantum machine learning framework Paddle Quantum 2.4.0³ as a development kit for constructing and training QNNs using numerical simulation. The implementation of our core logic consists of around 280 lines of Python code. Additionally, there are about 2600 lines of supporting code for evaluation purposes. All development and evaluation experiments for QuanTest were conducted on a computer with an Intel(R) Xeon(R) Gold 6146 CPU @ 3.20GHz processor with 12 cores, 256GB of memory, an NVIDIA GeForce RTX 2080 Ti GPU, and Ubuntu 18.04 as the host OS.

4.1 Research Questions

We summarize research questions to show QuanTest’s performance and effectiveness, which are listed as follows.

- **RQ1:** How effective is QuanTest in capturing the erroneous behaviors of QNN?
- **RQ2:** How is the quality of quantum adversarial examples generated by QuanTest?
- **RQ3:** How is the effectiveness of entanglement guidance for quantum adversarial testing?

To demonstrate the efficacy of QuanTest in capturing erroneous behaviors of QNN systems, we conducted tests using QuanTest on 9 representative mainstream QNN models. Subsequently, an analysis was performed on the generation of test samples by QuanTest across varying numbers of iterations. Finally, we evaluated the performance of QuanTest in quantum systems with varying dimensions. To answer RQ2, we analyze the fidelity measure and trace distance of the test samples generated by QuanTest, without imposing any similarity constraints. To address RQ3, we conducted

²<https://github.com/am0x00/QuanTest>

³<https://github.com/PaddlePaddle/Quantum>

Table 1. Details of Datasets and QNN Models.

Dataset	Description	Classification Task	QNN Model	# Quantum Gates	# Trainable Parameters	Acc. (%)
MNIST	28×28 handwritten digit images, transformed into 16×16 through downscaling, and embedded into 8-qubit states using amplitude encoding.	Binary classification for images of digit 3 and 6	CCQC	200	200	98.68
			QCL	160	120	97.97
			QCNN	134	169	98.48
		Ternary classification for images of digit 0, 1 and 2	CCQC	200	200	88.63
			QCL	160	120	86.37
			QCNN	134	169	89.27
Fashion-MNIST	28×28 grayscale images, undergoing the same downscaling method and encoding processing as MNIST.	Binary classification for images of trouser and coat	CCQC	200	200	95.85
			QCL	160	120	96.75
			QCNN	134	169	95.05

control experiments pertaining to entanglement-guided settings and analyzed the performance of QuanTest under the guidance of QEA with different values of k .

4.2 Experiment Setup

As depicted in Table 1, we adopt two widely utilized public datasets and then set three classification tasks. For each classification task, we evaluate QuanTest on three QNN models with distinct architectures (i.e., a total of nine QNN systems). This allows us to cover various popular QNN variants and ensures the versatility of the experimental results. Each real-world dataset is encoded into quantum state data using the same downscaling method and quantum state encoding strategy. All QNN models used for evaluation are trained by us using encoded quantum state data.

4.2.1 Dataset. The MNIST [35] handwritten digit database is a widely used classic dataset in the field of deep learning. It has become a standard benchmark for classification tasks. The dataset consists of 60,000 training examples and 10,000 testing examples. Each digit is stored as a gray-scale image with a size of 28×28 pixels. The Fashion-MNIST [75] is a dataset of Zalando’s article images containing 60,000 gray-scale fashion images as a training set and 10,000 images for testing.

We slightly reduced the size of images in both datasets from 28×28 pixels to 16×16 pixels so that we can simulate the QNN system with moderate classical computing resources. Subsequently, we established three classification tasks based on these two datasets, including binary classification of digits 3 and 6 in MNIST (denoted as MNIST[3,6]), ternary classification of digits 0, 1, and 2 in MNIST (denoted as MNIST[0,1,2]), and binary classification of trousers and coats in Fashion-MNIST (denoted as Fashion[1,4]). The selection of datasets and corresponding classification tasks is determined after a comprehensive consideration of the current limitations on the available qubits and the widely used setup of classification tasks in the field of quantum machine learning.

4.2.2 QNN Models. Quantum Circuit Learning (QCL) [50] is a representative hybrid classical-quantum framework. It employs a quantum neural network composed of a nonlinear quantum encoding circuit for input data and a low-depth quantum variational circuit capable of learning tasks through iterative parameter optimization to accomplish machine learning tasks such as high-dimensional regression or classification.

Circuit-centric quantum classifiers (CCQC) [62] is a low-depth hybrid quantum neural network framework designed for supervised learning, which leverages the entangling properties of quantum circuits to capture the correlations within data and achieve classification tasks.

Quantum Convolutional Neural Network (QCNN) [13] is a promising quantum neural network architecture inspired by classical convolutional neural networks. It primarily consists of convolutional layers, pooling layers, and fully connected layers implemented using parameterized quantum circuits. QCNN is considered a promising architecture due to the absence of barren plateaus [58].

4.2.3 Data Encoding. Quantum neural networks employ quantum states as input. Therefore, when they are utilized to analyze classical data, we need first to consider an appropriate quantum state representation for classical world data in the quantum system. This is achieved through quantum state encoding, which implements a feature map from classical bits in an N -dimensional Euclidean space to n qubits residing in a 2^n -dimensional Hilbert space: $\mathbb{R}^N \rightarrow \mathbb{C}^{2^n}$, completes the embedding of classical data into quantum states. There are several common strategies for quantum state encoding [28, 34, 61, 63]. To circumvent the challenges faced by traditional computers in numerically simulating a large number of qubits, in this work, we exclusively focus on processing the adopted dataset through amplitude encoding.

Amplitude encoding maps the feature information of classical data to the amplitudes of quantum states. For the input classical data $\mathbf{x} \in \mathbb{R}^N$, its vector elements are encoded and mapped to the amplitudes of $\lceil \log_2 N \rceil$ qubits: $|\mathbf{x}\rangle = \sum_{i=1}^N x_i |i\rangle$, where $\{|i\rangle\}$ represents a set of computational basis states in the Hilbert space. Since the feature information of classical data is represented as the amplitudes of a quantum state, the classical input must satisfy the normalization condition: $\|\mathbf{x}\|^2 = \sum_i |x_i|^2 = 1$. We require the use of 256 amplitudes of the 8-qubit system to encode this data information, as each image in the MNIST and Fashion-MNIST datasets is two dimensional and contains 16×16 pixels. Note that QunTest also possesses universality and extensibility for other encoding strategies.

4.2.4 Test Samples Generation. We use adversarial attack strategies FGSM [20] and DLFuzz [21] under the premise of an entanglement-guided approach to search for erroneous behaviors and generate quantum adversarial examples, for testing QNN models on the MNIST and Fashion-MNIST datasets encoded as quantum states. We have adapted these adversarial attack strategies with quantum-based adjustments to enable them to process quantum state inputs and the information extracted within QNN systems. Essentially, both of these strategies rely on a gradient-based manner to solve the optimization problem. These adversarial examples have imperceptible perturbations that are difficult for humans to detect, and demonstrate considerable effectiveness in revealing robustness issues in QNN systems.

In addition, we have prepared random noise samples generated by applying random coherent noise to original samples for subsequent comparative evaluation. We realized coherent noise by constructing a universal quantum rotation gate with Gaussian noise perturbation on the rotation parameters. This allows us to apply it as a random perturbation operator $U_\Delta(\sigma)$ on quantum original samples in the form of a quantum circuit, where σ represents the strength of the noise, reflecting the magnitude of the standard deviation in the normal distribution.

4.3 Capabilities of Erroneous Behavior Detection

To address the **RQ1**, we first compared our QunTest method with a strategy based on random coherent noise on multiple tested models. We randomly selected 800 original samples for each class category in the binary and ternary classification tasks of the MNIST and the binary classification task of Fashion-MNIST. These samples were used to generate adversarial and random noise samples. For the generation of quantum adversarial examples, we set all hyperparameters in the adversarial attack strategy to 1. We utilize QEA with $k = 1$ as guidance, and the weight selected for joint optimization is set to $w = 1$. For the generation of random noise samples, We set the noise strength in the random perturbation operator as $\sigma = 0.02$. Then, we choose a high standard for evaluating

Table 2. Capability of QuanTest to capture erroneous behaviors based on different adversarial attack strategies.

Data	Model	Gen_Rate(%)			AFM(%)			ATD		
		Random	QuanTest (FGSM-based)	QuanTest (DLFuzz-based)	Random	QuanTest (FGSM-based)	QuanTest (DLFuzz-based)	Random	QuanTest (FGSM-based)	QuanTest (DLFuzz-based)
Fashion[1,4]	CCQC	0.62	73.57	87.79	97.58	93.65	93.52	0.2143	0.3376	0.3428
	QCL	0.83	75.84	96.48	94.29	93.60	93.90	0.3138	0.3394	0.3327
	QCNN	2.49	79.94	92.73	95.80	95.09	95.07	0.2669	0.2924	0.2947
MNIST[0,1,2]	CCQC	3.15	44.52	70.95	95.65	95.28	95.06	0.2792	0.2775	0.2852
	QCL	3.74	56.17	71.52	95.40	95.55	96.26	0.2843	0.2677	0.2467
	QCNN	4.58	69.71	79.24	95.36	97.22	97.41	0.2827	0.2058	0.1984
MNIST[3,6]	CCQC	1.02	70.42	88.44	93.13	94.35	94.54	0.3611	0.3153	0.3117
	QCL	2.26	59.00	91.70	95.24	94.76	95.44	0.2800	0.3540	0.2811
	QCNN	0.82	84.59	96.87	93.85	94.95	95.29	0.3398	0.2963	0.2881

similarity with fidelity measure > 90% or trace distance < 0.45 to determine the qualification of the test samples, given the extensive Hilbert space dimensions of the QNN system. We ran the experiments three times on each tested model and took the average, to mitigate potential uncertainties in the results. In the absence of additional declarations, other evaluations default to the same predefined configuration.

Table 2 shows the overall results obtained with QuanTest and random coherent noise, where Gen Rate represents the test sample generation rate. The best performance is typeset in bold. Test samples generated by each strategy exhibit comparable similarities, as restrictions are imposed on the similarity metrics. The maximum difference for AFM does not exceed 3.89%, and for ATD, it does not exceed 0.14. This allows the evaluation of the test sample generation rates for each strategy with minimal interference. It can be observed that the test sample generation rate of coherent noise is generally low, reaching a maximum of only 4.58%. In contrast, QuanTest achieves a maximum test sample generation rate of 84.59% using the FGSM attack strategy, while the use of the DLFuzz attack strategy can result in a success rate of up to 96.87%. The test sample generation rate of the DLFuzz strategy is 9.53% to 26.43% higher than that of the FGSM strategy across various models.

Therefore, it can be concluded that QuanTest’s ability to capture erroneous behaviors is significantly higher under similar levels of similarity compared to the random coherent noise used as the baseline, and the adversarial attack strategies based on DLFuzz often generate more test samples. Note that the performance of QNN models in the presence of coherent noise also demonstrates its significant robustness to quantum stochastic noise itself. Models with better pre-training (The accuracy is shown in Table 1) exhibit stronger resistance to coherent noise. In addition, we observe a certain negative correlation between the model’s resistance to coherent noise and its performance in QuanTest (Pearson correlation coefficient of -0.74 for the test sample generation rate). This may imply that QuanTest is more capable of identifying deeper, atypical security issues in QNN systems.

Subsequently, we calculated the test sample generation rate under different iteration counts using the entanglement-guided DLFuzz strategy when no similarity constraints were imposed (i.e., Gen Rate=100%), as shown in Figure 6. The results indicate that QuanTest based on the DLFuzz strategy is capable of generating the majority of adversarial examples after 5-10 iterations. In contrast, QuanTest based on the FGSM strategy requires slightly more iterations. This may be related to the effectiveness of the adversarial attack strategy. In addition, the speed of test sample generation for QCNN is generally faster than other models, which may be related to the quality of the model construction.

We also investigate the performance of QuanTest in capturing erroneous behaviors in quantum systems of different dimensions. We used 784 amplitudes from the 10-qubit system to prepare quantum states for images of size 28×28 pixels in the dataset, with the last 240 bits of the state vector padded with zeros to ensure a length of 2¹⁰. We extended the pre-trained QNN model accordingly,

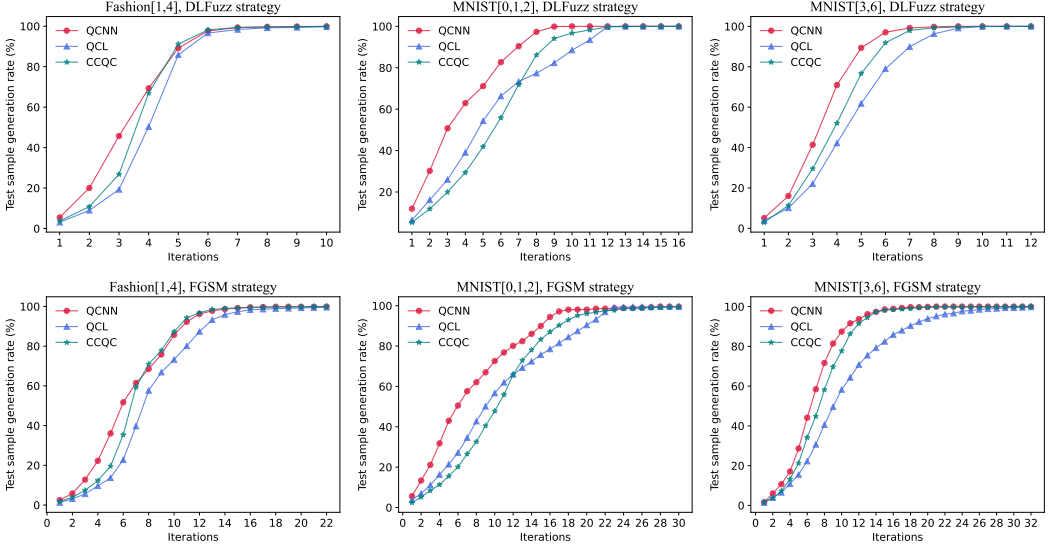


Fig. 6. Test sample generation rate of QuanTest at different iterations.

increasing the number of quantum gates and trainable parameters by 0.25 times due to the increase in the number of qubits. The training was terminated when the model achieved performance similar to the QNN model corresponding to 16×16 pixel images in the classification. This was done to ensure fairness in the comparative experiments. For each classification category in the classification task, we randomly selected 500 samples of size 16×16 pixels and 28×28 pixels. fidelity measure $> 95\%$ or trace distance < 0.30 were chosen as the criteria for adversarial example detection.

Table 3 shows the QuanTest’s performance using the DLFuzz strategy on samples of 16×16 pixels and the corresponding samples of 28×28 pixels. The best result across each row is denoted in bold. The results indicate that, under the same similarity constraints, QuanTest tends to generate more test samples for quantum systems with higher dimensions. This finding also partially confirms the theoretical proof by Liu and Wittek, demonstrating that a disturbance inversely proportional to the dimension is sufficient to cause a QNN system to induce a misclassification [38].

Answer to RQ1: QuanTest is capable of effectively capturing erroneous behaviors in QNN systems. It can efficiently generate a sufficient number of test samples with slight perturbations and performs better in quantum systems with higher dimensions.

4.4 Quality of Generated adversarial examples

To address the **RQ2**, we conducted a statistical analysis of the fidelity measure and trace distance between the quantum adversarial examples generated by QuanTest using different adversarial attack strategies and the quantum original samples. QuanTest generated 600 adversarial examples for each classification task without imposing any similarity constraints. In other words, we assessed the quality of the adversarial examples generated by QuanTest under the condition of Gen Rate=100%. This condition setting enables our statistics to cover a wide range of scenarios, including extreme cases, thereby enhancing the comprehensiveness of the evaluation.

Table 3. Performance of QuanTest based on the DLFuzz strategy in capturing erroneous behaviors in quantum systems of different dimensions.

Performance	Model	Data	Dimension	
			16 × 16	28 × 28
Gen_Rate(%)	CCQC	Fashion[1,4]	26.87	84.90
		MNIST[0,1,2]	30.59	82.91
		MNIST[3,6]	47.75	87.50
	QCL	Fashion[1,4]	37.78	70.14
		MNIST[0,1,2]	46.51	59.82
		MNIST[3,6]	65.30	78.72
	QCNN	Fashion[1,4]	39.20	89.29
		MNIST[0,1,2]	53.55	97.82
		MNIST[3,6]	53.78	94.33
AFM(%)	CCQC	Fashion[1,4]	96.94	96.89
		MNIST[0,1,2]	96.92	98.01
		MNIST[3,6]	97.26	98.58
	QCL	Fashion[1,4]	97.79	97.79
		MNIST[0,1,2]	97.96	98.40
		MNIST[3,6]	98.45	98.52
	QCNN	Fashion[1,4]	97.18	97.63
		MNIST[0,1,2]	97.37	98.13
		MNIST[3,6]	97.22	97.75
ATD	CCQC	Fashion[1,4]	0.2344	0.2367
		MNIST[0,1,2]	0.2349	0.1914
		MNIST[3,6]	0.2227	0.1622
	QCL	Fashion[1,4]	0.1922	0.1950
		MNIST[0,1,2]	0.1835	0.1629
		MNIST[3,6]	0.1606	0.1560
	QCNN	Fashion[1,4]	0.2269	0.2057
		MNIST[0,1,2]	0.2164	0.1808
		MNIST[3,6]	0.2241	0.1998

Figure 7 presents the value range of fidelity measure and trace distance obtained by different methods on each classification task respectively. The solid coral line corresponds to the median, while the dashed green line signifies the mean (i.e., AFM and ATD). We can observe that the fidelity measure of adversarial examples generated by QuanTest based on the DLFuzz strategy is generally higher than 85%, and the trace distance is generally lower than 0.6. The performance of using the FGSM strategy is slightly less favorable than the DLFuzz strategy, but the fidelity is generally above 80%, and the trace distance is generally below 0.8. Both strategies exhibit similar statistical patterns overall. The differences in the quality of test samples generated by different models based on the two strategies are also consistent with the differences in the iteration counts shown in Figure 6.

In fact, 80% is still a relatively high fidelity, given that the Hilbert space dimension of the QNN model is already very large. Therefore, whether using the DLFuzz or FGSM strategy, the adversarial examples generated under the guidance of QEA exhibit remarkable performance on AFM and ATD. This implies that the majority of test samples generated by QuanTest can trigger erroneous behaviors in the QNN system by applying imperceptible perturbations. This also allows us to generate test samples using QEA guidance without needing to overly consider the additional distortion cost produced by the joint optimization process.

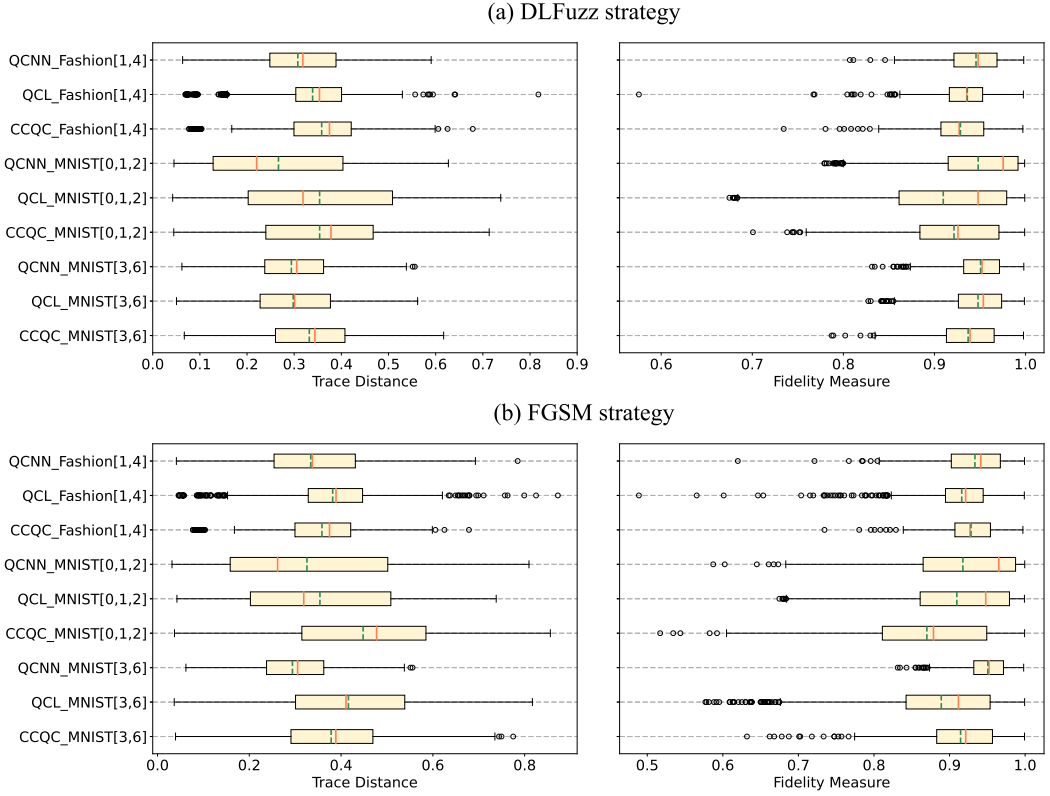


Fig. 7. Value range of trace distance and fidelity measure of adversarial examples generated by entanglement-guided adversarial attack strategies without imposing similarity constraints.

Answer to RQ2: The adversarial examples generated by QuanTest exhibit high quality and perform well in terms of both fidelity measure and trace distance.

4.5 Effectiveness of Entanglement Guidance

To address the **RQ3**, we first evaluated the performance of the tested model under two settings: with entanglement guidance and without entanglement guidance (i.e., pure adversarial attacks). In the absence of a similarity threshold, QuanTest randomly selected 600 original samples for each classification task to generate test samples, subjecting each quantum original sample to 5 iterations. We repeat each configuration 5 times and report the average results to mitigate randomness in the evaluation process.

Table 4 presents the overall performance of the DLFuzz strategy (denoted as \mathcal{D}) and FGSM strategy (denoted as \mathcal{F}) in QuanTest under settings with and without entanglement guidance (denoted as \mathcal{G}). We compare the performance of QuanTest when adopting the same adversarial attack strategy with or without the entanglement-guided settings, and highlight the better result in bold from the two scenarios. In the case of the FGSM strategy, the entanglement-guided setting can achieve an improvement of 5.15% to 10.00% in QEA, and the test sample generation rate can be increased by up to 14.84%. Similarly, in the case of the DLFuzz strategy, the entanglement-guided

Table 4. Performance of the adversarial testing with and without entanglement guidance.

Data	Model	Strategy	Performance			
			QEA(%) ($k = 1$)	Gen Rate(%)	AFM(%)	ATD
Fashion[1,4]	CCQC	\mathcal{D}	49.55	71.49	94.84	0.3061
		$\mathcal{D} + \mathcal{G}$	57.12	91.17	93.42	0.3452
		\mathcal{F}	51.39	11.78	99.00	0.1305
		$\mathcal{F} + \mathcal{G}$	57.88	19.60	97.41	0.2117
	QCL	\mathcal{D}	54.10	70.00	96.15	0.2587
		$\mathcal{D} + \mathcal{G}$	61.45	85.86	94.33	0.3212
		\mathcal{F}	55.44	10.88	99.21	0.1170
		$\mathcal{F} + \mathcal{G}$	62.12	13.69	98.04	0.1834
	QCNN	\mathcal{D}	38.08	75.31	97.07	0.2225
		$\mathcal{D} + \mathcal{G}$	44.84	89.22	95.28	0.2890
		\mathcal{F}	38.19	21.25	99.06	0.1272
		$\mathcal{F} + \mathcal{G}$	44.93	36.08	97.61	0.2049
MNIST[0,1,2]	CCQC	\mathcal{D}	16.25	33.11	98.98	0.1247
		$\mathcal{D} + \mathcal{G}$	24.53	41.90	97.32	0.2093
		\mathcal{F}	17.05	14.22	99.70	0.6983
		$\mathcal{F} + \mathcal{G}$	24.66	15.55	98.78	0.1401
	QCL	\mathcal{D}	19.93	48.60	98.85	0.1342
		$\mathcal{D} + \mathcal{G}$	28.00	54.33	97.37	0.2070
		\mathcal{F}	19.80	18.28	99.67	0.739
		$\mathcal{F} + \mathcal{G}$	26.82	21.39	98.81	0.1384
	QCNN	\mathcal{D}	18.09	69.34	98.66	0.1480
		$\mathcal{D} + \mathcal{G}$	22.89	71.14	98.00	0.1794
		\mathcal{F}	18.19	36.08	99.60	0.8282
		$\mathcal{F} + \mathcal{G}$	23.34	42.07	98.88	0.1364
MNIST[3,6]	CCQC	\mathcal{D}	19.93	55.33	96.92	0.2312
		$\mathcal{D} + \mathcal{G}$	28.07	76.65	95.10	0.2958
		\mathcal{F}	17.10	12.36	99.12	0.1263
		$\mathcal{F} + \mathcal{G}$	26.10	21.29	97.78	0.1973
	QCL	\mathcal{D}	21.32	60.37	98.34	0.1676
		$\mathcal{D} + \mathcal{G}$	31.79	61.80	96.98	0.2314
		\mathcal{F}	21.55	14.51	99.59	0.8431
		$\mathcal{F} + \mathcal{G}$	31.55	15.52	98.59	0.1553
	QCNN	\mathcal{D}	16.05	83.92	97.16	0.2213
		$\mathcal{D} + \mathcal{G}$	23.67	89.37	95.67	0.2773
		\mathcal{F}	15.34	18.39	99.16	0.1212
		$\mathcal{F} + \mathcal{G}$	23.34	28.63	98.06	0.1837

setting can achieve an improvement of 4.81% to 10.47% in QEA, with a maximum improvement of 21.32% in the test sample generation rate. In addition, settings with entanglement guidance also lead to lower similarity between the generated test samples and the original samples. Compared to settings without entanglement guidance, entanglement-guided settings reduce AFM by 0.65% to 1.82% and increase ATD by 0.29 to 0.85. The results indicate that, based on the same adversarial attack strategy, entanglement-guided configurations often lead to higher QEA and generate more

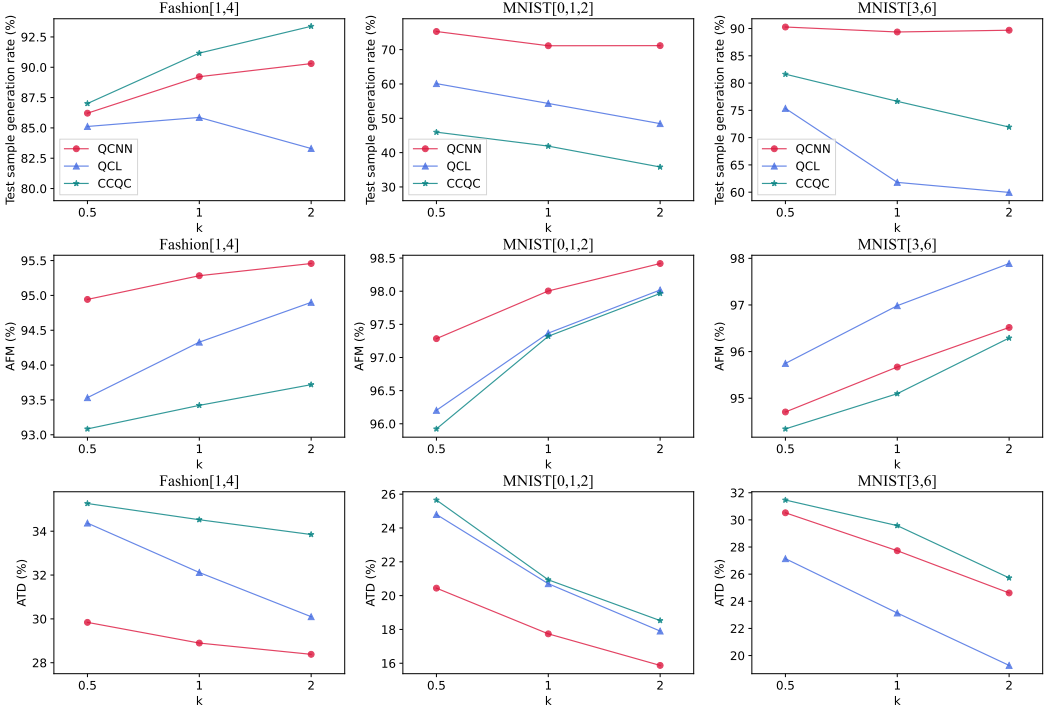


Fig. 8. Performance of QuanTest based on the DLFuzz strategy under the guidance of QEA at different values of k .

adversarial examples. Although entanglement guidance may introduce additional slight distortions, the marginal cost is entirely acceptable. Note that the increase in test sample generation rates brought about by entanglement-oriented settings cannot be achieved with the same small cost using random coherent noise.

In addition, we also assessed the performance of QuanTest based on the DLFuzz strategy under the guidance of QEA at different values of k . The magnitude of the k value can reflect the proportion of entanglement of the output quantum state in QEA. Similarly, we do not set a similarity limit and set the iteration count for each original sample to 5. We use the QEA's variant $QEA(k) = \frac{2k}{k+1} \cdot Q(U_{\Theta}|\mathbf{x}) - \frac{2}{k+1}Q(|\mathbf{x})$ as the optimization objective in the joint optimization process to avoid significant differences in the perturbation amounts generated by QEA at different k values, thereby avoiding interference with the evaluation. Figure 8 presents the overall results of the assessment.

For the MNIST dataset, the larger the k value of QEA, the fewer test sample generation rates it can achieve, while the Fashion dataset does not exhibit this property. The influence of QEA with different k values on the test sample generation rate further proves that entanglement guidance plays a role in generating adversarial examples. Another apparent phenomenon is that, with controlled perturbation levels, the smaller the k value of QEA, the lower the AFM of the generated test samples and the higher the ATD. This may be due to the concentration of entanglement measures of the output quantum state at higher values. This pattern also provides some reference for using QuanTest in the testing of QNN systems. When aiming to generate test samples with the highest possible similarity to the original samples, it may be advisable to consider appropriately increasing the value of k in QEA.

Answer to RQ3: Entanglement guidance can effectively traverse the solution space of QNN systems, discovering more erroneous behaviors. This capability is related to the proportion of entanglement of the output quantum state in QEA.

4.6 Threats to Validity

Quantum data encoding is a major threat to validity. Current classical computers can only simulate a limited number of qubits due to the enormous computational cost incurred by numerical simulations of high-dimensional quantum systems. Classical data is typically downsampled and then encoded into quantum states for training QNNs. We alleviate this threat by employing the Fashion and MNIST datasets, characterized by lower data dimensions.

Another threat could be the selection of QNN models. The construction of QNNs is still under exploration, and there exist various QNN variants based on different underlying architectures. To ensure the generalizability of QuanTest, we employ three different architectures of QNN models to evaluate QuanTest’s performance. We believe that QuanTest can be applied to the majority of PQC-based QNNs.

5 RELATED WORKS

5.1 Deep Learning Testing

Traditional black-box testing paradigms, such as manually labeled data and simulations, may not be able to discover various extreme cases that can lead to erroneous behaviors in machine learning systems. Pei et al. [57] innovatively proposed a white-box differential testing method, introducing neuron coverage as the first testing criterion to measure the extent to which the internal logic of DNN is being tested. Subsequently, several related testing works based on neuron coverage emerged. Deeptest [69] automatically generates test samples by applying various real image transformations (e.g., rotation and blurring) to maximize neuron coverage, and detect numerous potential defect behaviors in DNN-driven autonomous driving systems. DLFuzz [21] employs fuzzing into DL testing, and keeps minute mutation to the original samples, thereby maximizing the neuron coverage of mutated samples and the prediction differences from the quantum original samples.

Several new testing criteria have also been proposed since then. Deepgauge [43] proposed a set of more fine-grained neuron coverage criteria. DeepCT [42] introduced a set of coverage metrics for combinatorial testing based on neuron layers. However, the capacity of neuron coverage and its variants in test sample generation has also been questioned in some studies [23, 37]. In addition to coverage-guided testing, guiding testing using surprise adequacy [32] or robustness [70] have also been proposed, as well as some mutation testing [30, 44, 71] for DL systems. The unique features of RNN models make the work of RNN testing [16, 22, 39] distinctive. Deepstellar [16] abstracted an RNN into discrete-time Markov chain models and designed five coverage criteria based on this abstract model’s state transitions. RNN-Test [22] designed two coverage metrics for RNNs from the perspectives of state coverage. However, the work of QNN systems testing has garnered limited attention thus far. Due to its fundamentally different computational paradigm from classical computing, existing testing methods and criteria may not be suitable for it.

5.2 Adversarial Machine Learning

The vulnerability of machine learning models has garnered considerable attention [53, 68]. Attackers can deceive DNNs by applying imperceptible perturbations to input images. At present, there are plenty of works on conducting adversarial attacks on DL systems to generate adversarial examples

[11, 20, 33, 46, 51, 55]. adversarial examples existing in various input data such as images and text pose a broad threat to learning models [9, 56, 64].

In recent years, vulnerabilities to adversarial examples have also been found in quantum machine learning models [19, 41]. Quantum adversarial learning has been experimentally demonstrated on programmable superconducting qubits [60]. In contrast to these works, QuanTest systematically tests QNN systems by entanglement guidance. Moreover, QuanTest is exceptionally scalable and applicable to various PQC-based QNN systems and quantum state encoding strategies. Modularity allows QuanTest to directly achieve most quantum-adapted adversarial attack methods without the need for additional adjustments and adaptations, thus generating quantum adversarial examples with high efficiency.

5.3 Quantum Software Testing

With the rapid advancements in scale and reliability of quantum computing [1, 4, 5], the demand for quantum software development and testing is growing. Companies like Google⁴ and IBM⁵, while building their own quantum computers, have also introduced a range of quantum software development tools and quantum cloud platforms, such as Qiskit [14], PennyLane [8], Cirq [15], and TensorFlow Quantum [10]. These tools aim to assist engineers and researchers in developing quantum programs that can run on quantum computers.

At present, quantum software testing is largely still in its infancy. Due to the specialized characteristics of quantum computing, such as entanglement and superposition [54], quantum software testing faces challenges in various aspects, including state readout. Automated and systematic testing methods that can effectively scale for complex quantum programs on quantum computers are still missing due to factors like quantum noise, the scale of qubits, and underlying implementations. Most quantum software testing methods attempt to apply some of the testing techniques already existing in the classical world, such as differential testing [73], fuzz testing [72], mutation testing [17, 18, 47], and coverage criteria [2, 74], while making necessary adaptations to accommodate the inherent properties of quantum systems. Nevertheless, QNNs have a different programming paradigm and decision logic representation compared to traditional quantum software. Just as traditional software testing techniques could not be directly applied to classic DL systems, existing quantum software testing methods are equally inadequate for QNN systems.

6 CONCLUSION

In this paper, we propose QuanTest, an adversarial testing framework for QNN systems. QuanTest includes a set of similarity metrics and an entanglement adequacy criterion that can effectively detect erroneous behaviors in QNN systems under entanglement guidance, generating high-quality adversarial examples. Our experimental results demonstrate the effectiveness of QuanTest, where QuanTest is capable of generating several hundred times more test samples than random noise under equivalent perturbation size constraints. The average fidelity measure of these test samples consistently exceeds 95%.

REFERENCES

- [1] 2023. Suppressing quantum errors by scaling a surface code logical qubit. *Nature* 614, 7949 (2023), 676–681.
- [2] Shaukat Ali, Paolo Arcaini, Xinyi Wang, and Tao Yue. 2021. Assessing the Effectiveness of Input and Output Coverage Criteria for Testing Quantum Programs. In *2021 14th IEEE Conference on Software Testing, Verification and Validation (ICST)*. IEEE, 13–23.

⁴<https://quantumai.google/>

⁵<https://www.ibm.com/quantum>

- [3] Shaukat Ali and Tao Yue. 2023. Quantum Software Testing: A Brief Introduction. In *2023 IEEE/ACM 45th International Conference on Software Engineering: Companion Proceedings (ICSE-Companion)*. IEEE, 332–333.
- [4] Juan M Arrazola, Ville Bergholm, Kamil Brádler, Thomas R Bromley, Matt J Collins, Ish Dhand, Alberto Fumagalli, Thomas Gerrits, Andrey Goussev, Lukas G Helt, et al. 2021. Quantum circuits with many photons on a programmable nanophotonic chip. *Nature* 591, 7848 (2021), 54–60.
- [5] Philip Ball. 2021. First 100-QUBIT quantum computer enters crowded race. *Nature* 599 (2021), 542.
- [6] Johannes Bausch. 2020. Recurrent quantum neural networks. *Advances in neural information processing systems* 33 (2020), 1368–1379. <https://doi.org/10.48550/arXiv.2006.14619>
- [7] Marcello Benedetti, Erika Lloyd, Stefan Sack, and Mattia Fiorentini. 2019. Parameterized quantum circuits as machine learning models. *Quantum Science and Technology* 4, 4 (nov 2019), 043001. <https://doi.org/10.1088/2058-9565/ab4eb5>
- [8] Ville Bergholm, Josh A. Izaac, Maria Schuld, Christian Gogolin, and Nathan Killoran. 2018. PennyLane: Automatic differentiation of hybrid quantum-classical computations. *CoRR* abs/1811.04968 (2018). arXiv:1811.04968 <http://arxiv.org/abs/1811.04968>
- [9] Battista Biggio and Fabio Roli. 2018. Wild Patterns: Ten Years After the Rise of Adversarial Machine Learning. In *Proceedings of the 2018 ACM SIGSAC Conference on Computer and Communications Security (Toronto, Canada) (CCS '18)*. Association for Computing Machinery, New York, NY, USA, 2154–2156. <https://doi.org/10.1145/3243734.3264418>
- [10] Michael Broughton, Guillaume Verdon, Trevor McCourt, Antonio J Martinez, Jae Hyeon Yoo, Sergei V Isakov, Philip Massey, Ramin Halavati, Murphy Yuezhen Niu, Alexander Zlokapa, et al. 2020. Tensorflow quantum: A software framework for quantum machine learning. *arXiv preprint arXiv:2003.02989* (2020).
- [11] Nicholas Carlini and David Wagner. 2017. Towards evaluating the robustness of neural networks. In *2017 IEEE Symposium on Security and Privacy (SP)*. IEEE, 39–57.
- [12] Marco Cerezo, Andrew Arrasmith, Ryan Babbush, Simon C Benjamin, Suguru Endo, Keisuke Fujii, Jarrod R McClean, Kosuke Mitarai, Xiao Yuan, Lukasz Cincio, et al. 2021. Variational quantum algorithms. *Nature Reviews Physics* 3, 9 (aug 2021), 625–644. <https://doi.org/10.1038/s42254-021-00348-9>
- [13] Iris Cong, Soonwon Choi, and Mikhail D. Lukin. 2019. Quantum convolutional neural networks. *Nature Physics* 15, 12 (01 Dec 2019), 1273–1278. <https://doi.org/10.1038/s41567-019-0648-8>
- [14] Andrew Cross. 2018. The IBM Q experience and QISKit open-source quantum computing software. In *APS March meeting abstracts*, Vol. 2018. L58–003.
- [15] Cirq Developers. 2023. *Cirq*. <https://doi.org/10.5281/zenodo.8161252>
- [16] Xiaoning Du, Xiaofei Xie, Yi Li, Lei Ma, Yang Liu, and Jianjun Zhao. 2019. Deepstellar: Model-based quantitative analysis of stateful deep learning systems. In *Proceedings of the 2019 27th ACM Joint Meeting on European Software Engineering Conference and Symposium on the Foundations of Software Engineering*. 477–487.
- [17] Daniel Fortunato, José Campos, and Rui Abreu. 2022. Mutation testing of quantum programs written in QISKit. In *Proceedings of the ACM/IEEE 44th International Conference on Software Engineering: Companion Proceedings (Pittsburgh, Pennsylvania) (ICSE '22)*. Association for Computing Machinery, New York, NY, USA, 358–359. <https://doi.org/10.1145/3510454.3528649>
- [18] Daniel Fortunato, José Campos, and Rui Abreu. 2022. QMutPy: a mutation testing tool for Quantum algorithms and applications in Qiskit. In *Proceedings of the 31st ACM SIGSOFT International Symposium on Software Testing and Analysis (ISSTA 2022)*. Association for Computing Machinery, New York, NY, USA, 797–800. <https://doi.org/10.1145/3533767.3543296>
- [19] Weiyuan Gong and Dong-Ling Deng. 2022. Universal adversarial examples and perturbations for quantum classifiers. *National Science Review* 9, 6 (2022), nwab130.
- [20] Ian Goodfellow, Jonathon Shlens, and Christian Szegedy. 2015. Explaining and Harnessing Adversarial Examples. In *International Conference on Learning Representations*. IEEE, New York, NY, USA. <https://doi.org/10.48550/arXiv.1412.6572>
- [21] Jianmin Guo, Yu Jiang, Yue Zhao, Quan Chen, and Jianguang Sun. 2018. DLfuzz: Differential Fuzzing Testing of Deep Learning Systems. In *Proceedings of the 2018 26th ACM Joint Meeting on European Software Engineering Conference and Symposium on the Foundations of Software Engineering (Lake Buena Vista, FL, USA)*. Association for Computing Machinery, New York, NY, USA, 739–743. <https://doi.org/10.1145/3236024.3264835>
- [22] Jianmin Guo, Quan Zhang, Yue Zhao, Heyuan Shi, Yu Jiang, and Jia-Guang Sun. 2022. RNN-Test: Towards Adversarial Testing for Recurrent Neural Network Systems. *IEEE Trans. Software Eng.* 48, 10 (sep 2022), 4167–4180.
- [23] Fabrice Harel-Canada, Lingxiao Wang, Muhammad Ali Gulzar, Quanquan Gu, and Miryung Kim. 2020. Is neuron coverage a meaningful measure for testing deep neural networks?. In *Proceedings of the 28th ACM Joint Meeting on European Software Engineering Conference and Symposium on the Foundations of Software Engineering*. ACM, 851–862.
- [24] Aram W Harrow, Avinandan Hassidim, and Seth Lloyd. 2009. Quantum algorithm for linear systems of equations. *Physical review letters* 103, 15 (2009), 150502.

- [25] Vojtěch Havlíček, Antonio D Córcoles, Kristan Temme, Aram W Harrow, Abhinav Kandala, Jerry M Chow, and Jay M Gambetta. 2019. Supervised learning with quantum-enhanced feature spaces. *Nature* 567, 7747 (Mar 2019), 209–212. <https://doi.org/10.1038/s41586-019-0980-2>
- [26] Carl W. Helstrom. 1969. Quantum detection and estimation theory. *Journal of Statistical Physics* 1, 2 (01 Jun 1969), 231–252. <https://doi.org/10.1007/BF01007479>
- [27] Hsin-Yuan Huang, Michael Broughton, Jordan Cotler, Sitan Chen, Jerry Li, Masoud Mohseni, Hartmut Neven, Ryan Babbush, Richard Kueng, John Preskill, et al. 2022. Quantum advantage in learning from experiments. *Science* 376, 6598 (jun 2022), 1182–1186.
- [28] Hsin-Yuan Huang, Michael Broughton, Masoud Mohseni, Ryan Babbush, Sergio Boixo, Hartmut Neven, and Jarrod R. McClean. 2021. Power of data in quantum machine learning. *Nature communications* 12, 1 (feb 2021). <https://doi.org/10.1038/s41467-021-22539-9>
- [29] Yipeng Huang and Margaret Martonosi. 2019. Statistical assertions for validating patterns and finding bugs in quantum programs. In *Proceedings of the 46th International Symposium on Computer Architecture (ISCA '19)*. Association for Computing Machinery, New York, NY, USA, 541–553. <https://doi.org/10.1145/3307650.3322213>
- [30] Nargiz Humbatova, Gunel Jahangirova, and Paolo Tonella. 2021. DeepCrime: mutation testing of deep learning systems based on real faults. In *Proceedings of the 30th ACM SIGSOFT International Symposium on Software Testing and Analysis (Virtual, Denmark) (ISSTA 2021)*. Association for Computing Machinery, New York, NY, USA, 67–78. <https://doi.org/10.1145/3460319.3464825>
- [31] Richard Jozsa. 1994. Fidelity for Mixed Quantum States. *Journal of Modern Optics* 41, 12 (1994), 2315–2323. <https://doi.org/10.1080/09500349414552171> arXiv:<https://doi.org/10.1080/09500349414552171>
- [32] Jinhan Kim, Robert Feldt, and Shin Yoo. 2019. Guiding deep learning system testing using surprise adequacy. In *2019 IEEE/ACM 41st International Conference on Software Engineering (ICSE)*. IEEE, 1039–1049.
- [33] Alexey Kurakin, Ian J Goodfellow, and Samy Bengio. 2018. Adversarial examples in the physical world. In *Artificial intelligence safety and security*. Chapman and Hall/CRC, 99–112.
- [34] Ryan LaRose and Brian Coyle. 2020. Robust data encodings for quantum classifiers. *Phys. Rev. A* 102 (sep 2020), 032420. Issue 3. <https://doi.org/10.1103/PhysRevA.102.032420>
- [35] Yann LeCun, Corinna Cortes, and CJ Burges. 2010. MNIST handwritten digit database. *ATT Labs [Online]*. Available: <http://yann.lecun.com/exdb/mnist> (2010).
- [36] Gushu Li, Li Zhou, Nengkun Yu, Yufei Ding, Mingsheng Ying, and Yuan Xie. 2020. Projection-based runtime assertions for testing and debugging Quantum programs. *Proc. ACM Program. Lang.* 4, OOPSLA, Article 150 (nov 2020), 29 pages. <https://doi.org/10.1145/3428218>
- [37] Zenan Li, Xiaoxing Ma, Chang Xu, and Chun Cao. 2019. Structural coverage criteria for neural networks could be misleading. In *ICSE (NIER) (Montreal, QC, Canada)*. IEEE / ACM, 89–92. <https://doi.org/10.1109/ICSE-NIER.2019.00031>
- [38] Nana Liu and Peter Wittek. 2020. Vulnerability of quantum classification to adversarial perturbations. *Phys. Rev. A* 101 (jun 2020), 062331. Issue 6. <https://doi.org/10.1103/PhysRevA.101.062331>
- [39] Zixi Liu, Yang Feng, Yining Yin, and Zhenyu Chen. 2022. DeepState: selecting test suites to enhance the robustness of recurrent neural networks. In *Proceedings of the 44th International Conference on Software Engineering*. 598–609.
- [40] Seth Lloyd, Masoud Mohseni, and Patrick Rebentrost. 2014. Quantum principal component analysis. *Nature Physics* 10, 9 (2014), 631–633.
- [41] Sirui Lu, Lu-Ming Duan, and Dong-Ling Deng. 2020. Quantum adversarial machine learning. *Physical Review Research* 2, 3 (jan 2020), 033212. <https://doi.org/10.1103/PhysRevResearch.2.033212>
- [42] Lei Ma, Felix Juefei-Xu, Minhui Xue, Bo Li, Li Li, Yang Liu, and Jianjun Zhao. 2019. DeepCT: Tomographic Combinatorial Testing for Deep Learning Systems. In *26th IEEE International Conference on Software Analysis, Evolution and Reengineering, SANER 2019, Hangzhou, China, February 24-27, 2019*. Xinyu Wang, David Lo, and Emad Shihab (Eds.). IEEE, 614–618. <https://doi.org/10.1109/SANER.2019.8668044>
- [43] Lei Ma, Felix Juefei-Xu, Fuyuan Zhang, Jiyuan Sun, Minhui Xue, Bo Li, Chunyang Chen, Ting Su, Li Li, Yang Liu, et al. 2018. Deepgauge: Multi-granularity testing criteria for deep learning systems. In *Proceedings of the 33rd ACM/IEEE international conference on automated software engineering*. 120–131.
- [44] Lei Ma, Fuyuan Zhang, Jiyuan Sun, Minhui Xue, Bo Li, Felix Juefei-Xu, Chao Xie, Li Li, Yang Liu, Jianjun Zhao, and Yadong Wang. 2018. DeepMutation: Mutation Testing of Deep Learning Systems. In *2018 IEEE 29th international symposium on software reliability engineering (ISSRE) (Memphis, TN, USA)*. IEEE Computer Society, 100–111. <https://doi.org/10.1109/ISSRE.2018.00021>
- [45] Yanjun Ma, Dianhai Yu, Tian Wu, and Haifeng Wang. 2019. PaddlePaddle: An open-source deep learning platform from industrial practice. *Frontiers of Data and Computing* 1, 1 (2019), 105–115.
- [46] Aleksander Madry, Aleksandar Makelov, Ludwig Schmidt, Dimitris Tsipras, and Adrian Vladu. 2017. Towards deep learning models resistant to adversarial attacks. (2017). arXiv:[arXiv preprint arXiv:1706.06083](https://arxiv.org/abs/1706.06083)

- [47] Eñaut Mendiluze, Shaukat Ali, Paolo Arcaini, and Tao Yue. 2021. Muskit: A mutation analysis tool for quantum software testing. In *2021 36th IEEE/ACM International Conference on Automated Software Engineering (ASE)*. IEEE, 1266–1270.
- [48] David A. Meyer and Nolan R. Wallach. 2002. Global entanglement in multiparticle systems. *J. Math. Phys.* 43, 9 (aug 2002), 4273–4278. <https://doi.org/10.1063/1.1497700>
- [49] Andriy Miranskyy and Lei Zhang. 2019. On testing quantum programs. In *Proceedings of the 41st International Conference on Software Engineering: New Ideas and Emerging Results (Montreal, Quebec, Canada) (ICSE-NIER '19)*. IEEE Press, 57–60. <https://doi.org/10.1109/ICSE-NIER.2019.00023>
- [50] K. Mitarai, M. Negoro, M. Kitagawa, and K. Fujii. 2018. Quantum circuit learning. *Phys. Rev. A* 98 (sep 2018), 032309. Issue 3. <https://doi.org/10.1103/PhysRevA.98.032309>
- [51] Seyed-Mohsen Moosavi-Dezfooli, Alhussein Fawzi, and Pascal Frossard. 2016. DeepFool: A Simple and Accurate Method to Fool Deep Neural Networks. In *CVPR*. IEEE Computer Society, 2574–2582.
- [52] Asmar Muqet, Tao Yue, Shaukat Ali, and Paolo Arcaini. 2023. Noise-Aware Quantum Software Testing. (2023). <https://doi.org/10.48550/arXiv.2306.16992> arXiv:arXiv preprint arXiv:2306.16992
- [53] Anh Mai Nguyen, Jason Yosinski, and Jeff Clune. 2015. Deep neural networks are easily fooled: High confidence predictions for unrecognizable images. In *CVPR*. IEEE Computer Society, 427–436.
- [54] Michael A Nielsen and Isaac L Chuang. 2010. *Quantum computation and quantum information*. Cambridge university press. <https://doi.org/10.1017/CBO9780511976667>
- [55] Nicolas Papernot, Patrick McDaniel, Somesh Jha, Matt Fredrikson, Z Berkay Celik, and Ananthram Swami. 2016. The limitations of deep learning in adversarial settings. In *2016 IEEE European symposium on security and privacy (EuroS&P)*. IEEE, 372–387.
- [56] Nicolas Papernot, Patrick D. McDaniel, Ananthram Swami, and Richard E. Harang. 2016. Crafting adversarial input sequences for recurrent neural networks. In *MILCOM 2016-2016 IEEE Military Communications Conference*. IEEE, 49–54.
- [57] Kexin Pei, Yinzhi Cao, Junfeng Yang, and Suman Jana. 2017. Deepxplore: Automated whitebox testing of deep learning systems. In *proceedings of the 26th Symposium on Operating Systems Principles*. 1–18.
- [58] Arthur Pesah, M. Cerezo, Samson Wang, Tyler Volkoff, Andrew T. Sornborger, and Patrick J. Coles. 2021. Absence of Barren Plateaus in Quantum Convolutional Neural Networks. *Phys. Rev. X* 11 (oct 2021), 041011. Issue 4. <https://doi.org/10.1103/PhysRevX.11.041011>
- [59] Evan Peters, João Caldeira, Alan Ho, Stefan Leichenauer, Masoud Mohseni, Hartmut Neven, Panagiotis Spentzouris, Doug Strain, and Gabriel N Perdue. 2021. Machine learning of high dimensional data on a noisy quantum processor. *npj Quantum Information* 7, 1 (nov 2021), 161. <https://doi.org/10.1038/s41534-021-00498-9>
- [60] Wenhui Ren, Weikang Li, Shibo Xu, Ke Wang, Wenjie Jiang, Feitong Jin, Xuhao Zhu, Jiachen Chen, Zixuan Song, Pengfei Zhang, et al. 2022. Experimental quantum adversarial learning with programmable superconducting qubits. *Nature Computational Science* 2, 11 (apr 2022), 711–717. <https://doi.org/10.1038/s43588-022-00351-9>
- [61] Maria Schuld. 2021. Supervised quantum machine learning models are kernel methods. <https://doi.org/10.48550/arXiv.2101.11020> arXiv:2101.11020 [quant-ph]
- [62] Maria Schuld, Alex Bocharov, Krysta M. Svore, and Nathan Wiebe. 2020. Circuit-centric quantum classifiers. *Phys. Rev. A* 101 (mar 2020), 032308. Issue 3. <https://doi.org/10.1103/PhysRevA.101.032308>
- [63] Maria Schuld and Francesco Petruccione. 2018. *Information Encoding*. Springer International Publishing, Cham, 139–171. https://doi.org/10.1007/978-3-319-96424-9_5
- [64] Mahmood Sharif, Sruti Bhagavatula, Lujo Bauer, and Michael K. Reiter. 2016. Accessorize to a Crime: Real and Stealthy Attacks on State-of-the-Art Face Recognition. In *Proceedings of the 2016 acm sigsac conference on computer and communications security*. ACM, 1528–1540.
- [65] Jinjing Shi, Wenxuan Wang, Xiaoping Lou, Shichao Zhang, and Xuelong Li. 2022. Parameterized Hamiltonian learning with quantum circuit. *IEEE Transactions on Pattern Analysis and Machine Intelligence* 45, 5 (Aug 2022), 6086–6095.
- [66] Sukin Sim, Peter D Johnson, and Alán Aspuru-Guzik. 2019. Expressibility and entangling capability of parameterized quantum circuits for hybrid quantum-classical algorithms. *Advanced Quantum Technologies* 2, 12 (2019), 1900070. <https://doi.org/10.1002/qute.201900070>
- [67] Christian Szegedy, Wojciech Zaremba, Ilya Sutskever, Joan Bruna, Dumitru Erhan, Ian Goodfellow, and Rob Fergus. 2013. Intriguing properties of neural networks. (2013). <https://doi.org/10.48550/arXiv.1312.6199> arXiv:arXiv preprint arXiv:1312.6199
- [68] Christian Szegedy, Wojciech Zaremba, Ilya Sutskever, Joan Bruna, Dumitru Erhan, Ian J. Goodfellow, and Rob Fergus. 2014. Intriguing properties of neural networks. In *ICLR (Poster)*.
- [69] Yuchi Tian, Kexin Pei, Suman Jana, and Baishakhi Ray. 2018. Deeptest: Automated testing of deep-neural-network-driven autonomous cars. In *Proceedings of the 40th international conference on software engineering*. 303–314.

- [70] Jingyi Wang, Jialuo Chen, Youcheng Sun, Xingjun Ma, Dongxia Wang, Jun Sun, and Peng Cheng. 2021. RobOT: Robustness-oriented testing for deep learning systems. In *2021 IEEE/ACM 43rd International Conference on Software Engineering (ICSE)*. IEEE, 300–311.
- [71] Jingyi Wang, Guoliang Dong, Jun Sun, Xinyu Wang, and Peixin Zhang. 2019. Adversarial sample detection for deep neural network through model mutation testing. In *Proceedings of the 41st International Conference on Software Engineering (Montreal, Quebec, Canada) (ICSE '19)*. IEEE Press, 1245–1256. <https://doi.org/10.1109/ICSE.2019.00126>
- [72] Jiyuan Wang, Fucheng Ma, and Yu Jiang. 2021. Poster: Fuzz testing of quantum program. In *2021 14th IEEE Conference on Software Testing, Verification and Validation (ICST)*. IEEE, 466–469.
- [73] Jiyuan Wang, Qian Zhang, Guoqing Harry Xu, and Miryung Kim. 2022. QDiff: differential testing of quantum software stacks. In *Proceedings of the 36th IEEE/ACM International Conference on Automated Software Engineering (Melbourne, Australia) (ASE '21)*. IEEE Press, 692–704. <https://doi.org/10.1109/ASE51524.2021.9678792>
- [74] Xinyi Wang, Paolo Arcaini, Tao Yue, and Shaikat Ali. 2022. Quito: a coverage-guided test generator for quantum programs. In *Proceedings of the 36th IEEE/ACM International Conference on Automated Software Engineering (Melbourne, Australia) (ASE '21)*. IEEE Press, 1237–1241. <https://doi.org/10.1109/ASE51524.2021.9678798>
- [75] Han Xiao, Kashif Rasul, and Roland Vollgraf. 2017. Fashion-MNIST: a Novel Image Dataset for Benchmarking Machine Learning Algorithms. *CoRR abs/1708.07747* (2017). arXiv:1708.07747 <http://arxiv.org/abs/1708.07747>